J Mol Model (2009) 15:537–550
DOI 10.1007/s00894-008-0389-6

ORIGINAL PAPER

Conformational and electronic (AIM/NBO) study of unsubstituted A-type dimeric proanthocyanidin

Rosana M. Lobayan · Alicia H. Jubert · Martín G. Vitale · Alicia B. Pomilio

Received: 29 September 2008 / Accepted: 3 November 2008 / Published online: 19 December 2008

Abstract The conformational space of the unsubstituted A-type dimeric proanthocyanidin was scanned using molecular dynamics at a semiempirical level, and complemented with functional density calculations. The lowest energy conformers were obtained. Electronic distributions were analysed at a higher calculation level, thus improving the basis set. A topological study based on Bader's theory (AIM: atoms in molecules) and natural bond orbital (NBO) framework was performed. Furthermore, molecular electrostatic potential maps (MEPs) were obtained and analysed. NMR chemical shifts were calculated at ab initio level and further compared with previous experimental values; coupling constants were also calculated. The stereochemistry of the molecule is thoroughly discussed, revealing the key role that hyperconjugative interactions play in defining experimental trends. These results show the versatility of geminal spin–spin coupling ^{2}J(C-1′,O) as a probe for stereochemical studies of proanthocyanidins.

Keywords Atoms in molecules · Dimeric procyanidin · Density functional theory · Nuclear magnetic resonance · Natural bond orbital analysis · Topological properties

R. M. Lobayan (✉)
Facultad de Ingeniería, Universidad de la Cuenca del Plata,
Lavalle 50,
3400 Corrientes, Argentina
e-mail: rlobayan@arnet.com.ar

A. H. Jubert
CEQUINOR Facultad de Ciencias Exactas y Facultad de Ingeniería, Universidad Nacional de La Plata,
CC 962,
1900 La Plata, Argentina

M. G. Vitale
INIFTA (UNLP, CONICET), Facultad de Ciencias Exactas,
Universidad Nacional de La Plata,
1900 La Plata, Argentina

A. B. Pomilio
PRALIB (UBA, CONICET), Facultad de Farmacia y Bioquímica,
Universidad de Buenos Aires,
Junín 956,
C1113AAD Buenos Aires, Argentina

Introduction

Proanthocyanidins are naturally occurring organic compounds found in some vascular plants, and have been also synthesised with a variety of substituents on the aromatic rings [1]. Their antioxidant role is widely documented, but no crystallographic data are available [2–6]. One of the most important applications of proanthocyanidins is the stabilisation of suspensions, which is useful in food industry, mainly in developing citrus juices [1, 7].

Depending on the position of the ethereal bridge, the structure of dimeric procyanidins can be of A- or B-type (Fig. 1; where numbering is indicated).

The aim of this study was to analyse thoroughly the structure and stereochemistry of the unsubstituted A-type proanthocyanidin to address the lack of reports on the structure features of this molecule.

Furthermore, experimental and theoretical studies are of interest to obtain a more comprehensive knowledge of the structure and function relationship of this kind of flavonoids as food antioxidants. This paper attempts to elucidate deeper insights into their physicochemical molecular properties, and the effects of these compounds on oxidative processes, as a first step towards our aim of rationalising the action of dimeric procyanidins in juice stabilisation.

The problems of calculating magnetic shieldings within ab initio or density functional theory (DFT) have been overcome

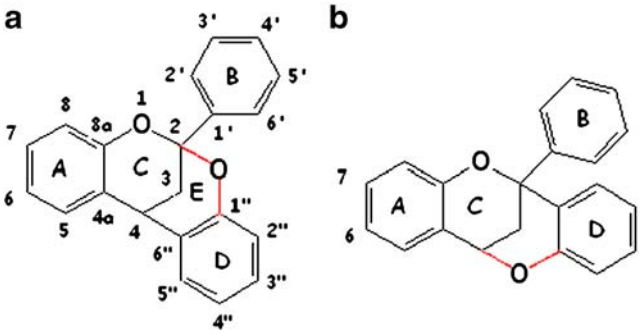

Fig. 1 Structures of unsubstituted A-type and B-type dimeric proanthocyanidins. Atom numbering is indicated

[8, 9]. Rapid progress has been made in developing techniques such as gauge invariant (or including) atomic orbitals (GIAO) [10, 11] or individual gauge for localized orbitals (IGLO) [12], which are able to calculate magnetic properties efficiently and relatively accurately. Furthermore, extensions of the original Hartree-Fock (HF) formalisms to second-order Møller-Plesset (MP2) [13] and DFT [11, 14] calculations improved the accuracy of the calculated values. Determination of chemical shifts by direct comparison of NMR experimental spectra remains a major use of ab initio and/or DFT magnetic shielding calculations. Usually, chemical shifts on the δ-scale are calculated by taking the difference between the calculated shielding and that found for a reference molecule, such as tetramethylsilane (TMS).

Through the study of molecular charge distribution (ρ) topology, AIM theory (Bader's theory of atoms in molecules) yields a single unified theory of molecular structure that defines atoms, bonds, structure, and mechanisms of structural changes, and also allows the Lewis standpoint of a chemical reaction to be followed in order to determine electrophilic and nucleophilic regions of a molecule from the topology and topography of the Laplacian of charge density, $\nabla^2\rho$ [15–17].

The conformational space of the stereoisomers of A-type procyanidin was scanned using molecular dynamics (MD) calculations, and further density calculations were performed to optimise the geometry of the lowest-energy conformers of each species obtained in the simulations. Nuclear magnetic resonance (NMR) chemical shifts were calculated at ab initio level and compared with previous experimental values. Molecular electrostatic potential maps (MEPs) were obtained and analysed, and topological analysis was performed in the frame of AIM together with natural bond orbital (NBO) analysis.

The results presented contribute to our understanding of the structure and stability of these compounds, in an analysis that aimed to describe, once substituted, its stabilisation and the possible interactions with other organic molecules present in a food matrix. Owing to the complexity of these structures (e.g. the occurrence of two prochiral carbons, and rigid [3.1.3] bicyclic substructure), the study of the conformational space of substituted and polymeric species, and the stability and reactivity of the lowest energy conformers, needs a deeper knowledge of unsubstituted procyanidins as a first step.

Methods

Conformational space for unsubstituted A-type dimeric proanthocyanidin stereoisomers was studied using the MD module of the HyperChem package [18]. Several simulations were accomplished at the AM1 level. Starting geometries were heated from 0 to 800 K in steps of 0.1 ps. Then, the temperature was kept constant by coupling the system to a simulated thermal bath with a bath relaxation time of 0.5 ps. The simulation time step was 0.5 fs. After an equilibration period of 1 ps, a 500 ps-long simulation was run, saving coordinates every 1 ps. Those geometries were then optimised to an energy gradient lower than 0.01 kcal mol^{-1} A^{-1} at the AM1 level.

Those conformers of lowest energy, obtained according to the methodology mentioned above (Fig. 2), were further studied using DFT as implemented in the Gaussian 98 package [19]. Geometry optimisations were performed using Becke's three parameters hybrid functional [20] with the Lee-Yang-Parr correlation functional [21], a combination that gives rise to the well known B3LYP method. The 6–31G** basis set was used for all atoms. Vibrational analysis was performed at the same level of theory as above for all optimised geometries in order to verify whether they were local minima or saddle points on the potential energy surface of the molecule. MEPs were calculated with the Gaussian package, and visual representations were obtained with the Molekel program [22].

^{13}C magnetic isotropic shielding tensors of the lowest-energy conformer of compounds were calculated using the GIAO method as implemented in the Gaussian 98 package at the same level of theory as above, i.e. B3LYP/6–31G**. Shielding tensors were converted to chemical shifts using TMS as a reference.

Topological analyses and evaluation of local properties were carried out with the PROAIM software [23] using the wave functions calculated at the B3LYP level and the 6–311++G** basis set implemented in the G98 computer program [19]. An NBO analysis was performed at the same level [24].

Results and discussion

Stereochemistry of unsubstituted A-type dimeric proanthocyanidin from an organic chemistry viewpoint

Unsubstituted A-type dimeric proanthocyanidin has two prochiral carbons, namely C-2 and C-4 (Fig. 1), as each of

these carbons has two identical and two different substituents. Just substituting one of the identical groups with another group different from the three attached to this prochiral carbon will result in formation of a chiral centre. Moreover, in this proanthocyanin, an asymmetric aromatic substitution in the A and D rings will also lead to a chiral compound. This A-type dimeric proanthocyanidin has an intramolecular plane of symmetry, thus indicating that this molecule is devoid of chirality. The occurrence of two C and E rings, and a CH_2-3 bridge markedly decreases the flexibility of the molecule. Therefore, the main substructure of this molecule is a [3.1.3]bicyclic structure, which consists of two six-membered C and E rings, each involved in a benzo-γ-pyrane, fused by a CH_2-3-containing bridge with C-2 and C-4 as head bridge carbons. Consequently, this bridge is a stereocentre, which gives rise to *E*/*Z*-isomerism, depending on the configuration of Ph-2 and H-4, or any other substituent present in these positions.

The *Z*-isomer accounts for both Ph-2 and H-4 being oriented towards the same face of the molecule plane, e.g. both Ph-2 and H-4 are upward oriented, β-oriented (*Re* face), with the other isomer having both substituents downward oriented, α-oriented (*Si* face). Due to the intramolecular plane of symmetry, and the molecule accommodation when changing substituent configuration, both possible *Z* structures are identical. Thus, there is only one *Z*-isomer.

Concerning the *E*-isomer, two geometric isomers are possible depending on the configuration of each substituent, e.g. Ph-2 and H-4. One of these isomers corresponds to βPh-2αH-4, and the other to αPh-2βH-4.

Moreover, the *Z*-isomer is likely to have rotamers due to rotation around the C-1′–C-2 bond. Scanning their conformational space revealed two conformers of lowest energy for the *Z*-isomer, and only one for the *E*-isomer: βPh-2αH-4. Geometry optimisations were performed at the B3LYP/6–31G** level and were confirmed as local minima by vibrational analysis, which was performed at the same level of calculation. Optimised conformers are shown in Fig. 2, e.g. Z-1 and Z-2 rotamers for *Z*-isomer, and one conformer, αPh-2βH-4, for *E*-isomer (abbreviated: αPhβH-E).

Relevant internal coordinates (angles and dihedral angles) of the lowest energy conformers of the unsubstituted A-type dimeric proanthocyanidin are listed in Table 1. Bond lengths are shown in Tables 2 and 3. The corresponding energies are also reported. The three isomers have a high symmetry, and the spatial position of the A ring relative to the D ring is very similar in them all. The main difference relies on the C-3–C-2–C-1′ angle, which is 112.6° for Z-1, 116.4° for Z-2, and 220.4° for αPhβH-E.

Steric hindrance and high ring tension are characteristics of the *E*-isomer. Therefore this stereoisomer shows higher energy than the *Z*-isomer. Consequently the lowest energy conformers for Z-1 and Z-2 are more stable than that for αPhβH-E and will be analysed thoroughly.

The Z-1 conformer has the lowest energy and is characterised by a C-3–C-2–C-1′–C-6′ dihedral angle of 88.2°. This angle is 0.0° for the Z-2 conformer. The angles between bonds that define the C and E rings, and their lengths are very similar for both Z-1 and Z-2.

Although the C-3–C-2–C-1′ angle differs by approximately 4°, Z-2 can be considered as a rotamer of Z-1. Both Z-1 and Z-2 have the intramolecular symmetry plane mentioned above. C-2, C-4 and CH_2-3 are included in the plane of symmetry.

The C-2–CH_2-3–C-4 bridge maintains a rigid conformation due to bonding to both heteroatom-containing C and E rings, thus resembling a cyclopropane or a double bond. In fact, our measurements have demonstrated that the π-character of the bonds involved in this bridge is rather high. The contribution of atomic *p* orbitals from the C-3 atom to the C-2–C-3 and C-3–C-4 bonds accounts for 74.08% and 72.61%, respectively. These values are stronger than those of ethane, at 70.4% (see below).

Topology of the electronic charge density function and NBO analysis

AIM theory is based upon critical points (CPs) of the molecular charge density, ρ (r) [15–17, 25, 26]. At these points, the gradient of the electron density, $\nabla\rho(r)$, is null, and is characterised by three eigenvalues, λ_i (i=1, 2, 3), of the $\nabla^2\rho(r)$ Hessian matrix. CPs are named and classified as (*r*,*s*) according to their rank, *r* (number of non-zero eigenvalues), and signature, *s* (three eigenvalues algebraic sum). A (3, −3) point accounts for a local maximum in ρ(r), characterised by $\nabla^2\rho(r) < 0$, and regularly occurs only at nuclear positions (nuclear critical point, NCP). A (3, −1) critical point, or bond CP (BCP), is usually found within two neighbouring nuclei, indicating the existence of a bond between them. Several properties evaluated at BCP are useful tools in classifying a given chemical structure [26]. Two negative eigenvalues of the Hessian matrix (λ_1 and λ_2, respectively) measure the contraction extent of ρ(r) at a direction normal to the bond towards CP, while a positive eigenvalue (i.e. λ_3) gives a quantitative indication of the contraction extent parallel to the bond, and from CP towards each of the neighbouring nuclei. When negative eigenvalues dominate, electron charge is locally concentrated in the region of CP, leading to an interaction attributable to covalent or polarised bonds. These are characterised by large ρ(r) values, $\nabla^2\rho(r) < 0$, and $|\lambda_1|/\lambda_3 > 1$ and $G_{bb}<1$, G_b being local kinetic energy density at BCP. When positive eigenvalues dominate, electron density is concentrated locally at each atomic basin. Interaction is classified as closed shell and is typical of highly ionic

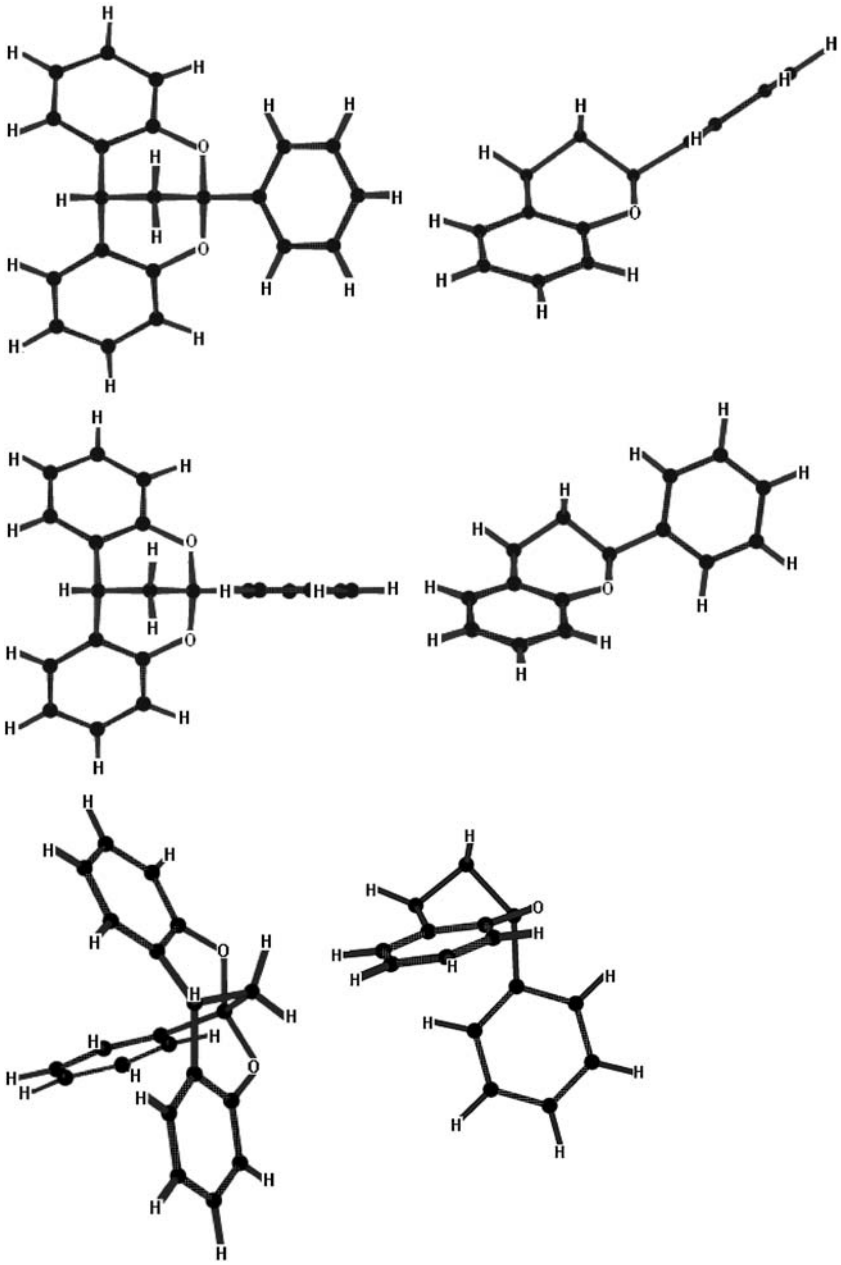

Fig. 2 Optimised geometry of both conformers of the Z-isomer of unsubstituted A-type dimeric proanthocyanidin at the B3LYP/6–31G** level. The E-isomer is also shown. Geometries are confirmed as local minimal by vibrational analysis

bonds, hydrogen bonds, and van der Waals interactions. This particular interaction is described by relatively low $\rho(r)$ values, $\nabla^2\rho(r) > 0$ and $|\lambda_1|/\lambda_3 < 1$, and $G_{bb}>1$. Another interesting parameter is ellipticity, ε, defined as $\lambda_1/\lambda_2 - 1$. Ellipticity is indicative of the similarity between perpendicular curvatures (λ_1 and λ_2) at BCP, and measures the extent to which density is preferentially accumulated in a given plane containing the bond path. If $\lambda_1=\lambda_2$, then $\varepsilon=0$, and the bond is cylindrically symmetric, e.g. a C–C single bond in ethane, and a triple bond in acetylene. Thus, in terms of the orbital model of electronic structure, ε is a measure of the π-character of the bonding up to the limit of "double bond" for which ellipticity reaches a maximum, further providing a quantitative measure for electron charge delocalisation [15].

Tables 2 and 3 show the most significant topological local properties at BCPs for the Z-1 and Z-2 conformers, e.g., density, ρ_b, Laplacian of the electron charge density, $\nabla^2\rho_b$, three eigenvalues λ_1, λ_2 and λ_3, ellipticity, ε, relationship between perpendicular and parallel curvatures, $|\lambda_1|/\lambda_3$, and kinetic energy density per charge unit, G_{bb}, for all bonds of Z-1 and Z-2, respectively. Bond lengths are also indicated in Tables 2 and 3. It is observed that all BCPs, except for BCP of the O1–C-8a bond, are characterised by large ρ_b values, $|\lambda_1|/\lambda_3 > 1$, and $G_{bb}<1$, which means that negative curvatures predominate and electron

Table 1 Relevant internal coordinates of the lowest energy conformers, and rotamers of unsubstituted A-type dimeric proanthocyanidin calculated at the B3LYP/6–31G** level

	Z-1	Z-2	αPhβH-E
ΔE	0.000	0.003	0.196
Dihedral angles:			
C_3–C_2–$C_{1'}$–$C_{6'}$	88.2	0.0	0.0
C_3–C_2–$C_{1'}$–$C_{2'}$	88.2	−180.0	180.0
O_1–C_2–$C_{1'}$–$C_{2'}$	33.5	−93.3	68.6
Angles:			
C_3–C_2–$C_{1'}$	112.6	116.4	220.4
C_2–C_3–C_4	107.5	107.4	94.0
C_{8a}–O_1–C_2	120.2	120.4	97.4
C_{4a}–C_4–$C_{6''}$	111.4	111.5	130.2
O_1–C_2–O	109.0	108.4	135.0
C_{4a}–C_{8a}–O_1	122.9	122.7	123.6
C_4–C_{4a}–C_{8a}	118.2	118.0	120.8
C_{4a}–C_4–C_3	107.8	108.0	95.5

Isomers refer to those in Fig. 2. Energy (Hartrees), bond lengths (Å), angles and dihedral angles (degrees)

charge is locally concentrated within the interatomic region, thus leading to an interaction characteristic of covalent polarised bonds. As the O1–C-8a bond have large ρ_b values, $\nabla^2\rho(r) < 0$, but $|\lambda_1|/\lambda_3<1$, and $G_{bb}>1$, is classified as an intermediate polar interaction. This attribute obeys the increase in positive eigenvalue of the Hessian matrix (Table 2) and indicates an increase in the contraction extent of ρ(r) parallel to the bond and from CP towards each of the neighbouring nuclei, although $\nabla^2\rho_b$ remains less than zero and ρ_b values are not low.

We found that this behaviour is typical of O–C bonds in pyrane rings, where the C atom also has an sp^2 hybridisation (ρ_b=0.274 a.u.,$\nabla^2\rho_b$=−0.304 a.u., λ_1=−0.523 a.u., λ_3=0.744 a.u., $|\lambda_1|/\lambda_3$=0.703 and G_b/ρ_b=1.111 a.u., for pyrane O–C studied at the same calculation level: B3LYP/6–31G**//B3LYP/6–311++G**). The decrease in the positive eigenvalue at BCP of O-1–C-2 bond and its characterisation as a typical covalent bond is explained by a C-2 (sp^3) hybridisation change when the γ-pyrane moiety is constituted. In fact, we also found that benzo-2,3-dihydro-

Table 2 Topological properties at bond critical point (BCP) (3,−1) in the Z-1 conformer calculated at the B3LYP/6–311++G** level of theory

		Bond length (Å)	ρ_b(a.u.)	$\nabla^2\rho_b$(a.u.)	λ_1	λ_2	λ_3	ε	G_b/ρ_b(a.u.)	$\lvert\lambda_1\rvert/\lambda_3$
A ring	C_{4a} – C_5	1.40	0.305	−0.830	−0.636	−0.522	0.327	0.219	0.329	1.944
	C_5 – C_6	1.39	0.308	−0.853	−0.646	−0.533	0.326	0.212	0.327	1.983
	C_6 – C_7	1.40	0.307	−0.848	−0.642	−0.533	0.327	0.204	0.322	1.961
	C_7 –C_8	1.39	0.308	−0.853	−0.646	−0.531	0.324	0.216	0.329	1.996
	C_8 – C_{8a}	1.40	0.310	−0.869	−0.662	−0.534	0.327	0.239	0.324	2.024
	C_{8a} – C_{4a}	1.40	0.307	−0.840	−0.650	−0.520	0.330	0.249	0.332	1.967
	C_5 – H	1.09	0.279	−0.951	−0.740	−0.726	0.515	0.021	0.139	1.437
	C_6 – H	1.08	0.280	−0.957	−0.746	−0.728	0.517	0.024	0.139	1.441
	C_7 – H	1.09	0.281	−0.962	−0.749	−0.735	0.521	0.019	0.135	1.436
	C_8 – H	1.08	0.280	−0.959	−0.752	−0.734	0.527	0.024	0.135	1.427
B ring	$C_{1'}$–$C_{2'}$	1.40	0.305	−0.834	−0.636	−0.527	0.329	0.207	0.326	1.932
	$C_{2'}$–$C_{3'}$	1.39	0.308	−0.856	−0.645	−0.537	0.327	0.201	0.324	1.974
	$C_{3'}$–$C_{4'}$	1.39	0.308	−0.858	−0.647	−0.539	0.327	0.200	0.322	1.975
	$C_{4'}$–$C_{5'}$	1.39	0.308	−0.858	−0.647	−0.539	0.327	0.200	0.322	1.975
	$C_{5'}$–$C_{6'}$	1.39	0.308	−0.856	−0.645	−0.537	0.327	0.201	0.324	1.974
	$C_{6'}$–$C_{1'}$	1.40	0.305	−0.834	−0.636	−0.527	0.329	0.207	0.326	1.932
	$C_{2'}$–*H*	1.08	0.283	−0.977	−0.763	−0.749	0.535	0.019	0.131	1.426
	$C_{3'}$–*H*	1.09	0.281	−0.961	−0.748	−0.734	0.520	0.019	0.136	1.437
	$C_{4'}$–*H*	1.09	0.281	−0.961	−0.747	−0.734	0.520	0.018	0.135	1.437
	$C_{5'}$–*H*	1.09	0.281	−0.961	−0.748	−0.734	0.520	0.019	0.136	1.437
	$C_{6'}$–*H*	1.08	0.283	−0.977	−0.763	−0.749	0.535	0.019	0.131	1.426
	$C_{1'}$–C_2	1.52	0.255	−0.624	−0.515	−0.484	0.374	0.064	0.211	1.376
C ring	O_1 – C_2	1.43	0.253	−0.521	−0.504	−0.456	0.438	0.106	0.752	1.149
	C_2 – C_3	1.53	0.248	−0.572	−0.477	−0.469	0.373	0.017	0.236	1.278
	C_3 – C_4	1.53	0.241	−0.534	−0.449	−0.445	0.360	0.010	0.235	1.246
	C_4 – C_{4a}	1.52	0.247	−0.565	−0.469	−0.454	0.358	0.032	0.238	1.310
	C_{4a} – C_{8a}	1.40	0.307	−0.840	−0.650	−0.520	0.330	0.249	0.332	1.967
	C_{8a} – O_1	1.38	0.274	−0.365	−0.527	−0.527	0.690	0.000	1.051	0.764
	C_3 – H	1.09	0.276	−0.923	−0.720	−0.717	0.514	0.004	0.147	1.401
	C_3 – H′	1.09	0.276	−0.923	−0.720	−0.717	0.514	0.004	0.147	1.401
	C_4 – H	1.09	0.276	−0.922	−0.719	−0.718	0.515	0.001	0.147	1.396

Isomers refer to those in Fig. 2

Table 3 Topological properties at BCP (3,−1) in the Z-2 conformer calculated at the B3LYP/6–311++G** level of theory

		Bond length (Å)	ρ_b(a.u.)	$\nabla^2\rho_b$(a.u.)	λ_1	λ_2	λ_3	ε	G_b/ρ_b(a.u.)	$\lvert\lambda_1\rvert/\lambda_3$
A ring	$C_{4a} - C_5$	1.40	0.305	−0.831	−0.636	−0.522	0.327	0.220	0.329	1.945
	$C_5 - C_6$	1.39	0.308	−0.853	−0.646	−0.533	0.326	0.213	0.327	1.984
	$C_6 - C_7$	1.40	0.306	−0.847	−0.642	−0.533	0.328	0.203	0.322	1.959
	$C_7 - C_8$	1.39	0.308	−0.854	−0.646	−0.531	0.323	0.216	0.329	1.998
	$C_8 - C_{8a}$	1.40	0.309	−0.868	−0.661	−0.534	0.327	0.239	0.324	2.020
	$C_{8a} - C_{4a}$	1.40	0.307	−0.841	−0.651	−0.521	0.331	0.249	0.332	1.969
	$C_5 - H$	1.09	0.279	−0.950	−0.740	−0.725	0.515	0.021	0.139	1.437
	$C_6 - H$	1.08	0.280	−0.956	−0.746	−0.728	0.517	0.025	0.139	1.442
	$C_7 - H$	1.09	0.281	−0.962	−0.748	−0.735	0.521	0.019	0.135	1.436
	$C_8 - H$	1.08	0.280	−0.960	−0.752	−0.735	0.527	0.024	0.134	1.427
B ring	C_r–$C_{2'}$	1.40	0.304	−0.831	−0.633	−0.529	0.331	0.198	0.322	1.913
	$C_{2'}$–$C_{3'}$	1.39	0.310	−0.865	−0.650	−0.540	0.325	0.205	0.327	1.998
	$C_{3'}$–$C_{4'}$	1.40	0.307	−0.853	−0.643	−0.538	0.328	0.195	0.320	1.958
	$C_{4'}$–$C_{5'}$	1.39	0.309	−0.864	−0.650	−0.540	0.326	0.205	0.325	1.993
	$C_{5'}$–$C_{6'}$	1.40	0.306	−0.848	−0.641	−0.535	0.328	0.200	0.321	1.956
	$C_{6'}$–$C_{1'}$	1.40	0.306	−0.836	−0.640	−0.524	0.328	0.220	0.330	1.952
	$C_{2'}$–*H*	1.08	0.283	−0.980	−0.764	−0.752	0.537	0.016	0.129	1.424
	$C_{3'}$–*H*	1.09	0.281	−0.962	−0.748	−0.735	0.521	0.019	0.135	1.436
	$C_{4'}$–*H*	1.09	0.281	−0.961	−0.748	−0.734	0.520	0.018	0.135	1.437
	$C_{5'}$–*H*	1.09	0.280	−0.960	−0.747	−0.733	0.519	0.020	0.136	1.438
	$C_{6'}$–*H*	1.08	0.282	−0.965	−0.749	−0.735	0.519	0.020	0.140	1.443
	$C1_{6'}$–$C_{2'}$	1.52	0.256	−0.630	−0.505	−0.499	0.374	0.011	0.210	1.351
C ring	$O_1 - C_2$	1.44	0.250	−0.517	−0.493	−0.449	0.425	0.096	0.729	1.159
	$C_2 - C_3$	1.53	0.251	−0.589	−0.485	−0.476	0.372	0.020	0.235	1.304
	$C_3 - C_4$	1.53	0.240	−0.531	−0.447	−0.443	0.359	0.009	0.235	1.244
	$C_4 - C_{4a}$	1.52	0.247	−0.567	−0.470	−0.455	0.358	0.032	0.238	1.312
	$C_{4a} - C_{8a}$	1.40	0.307	−0.841	−0.651	−0.521	0.331	0.249	0.332	1.969
	$C_{8a} - O_1$	1.38	0.275	−0.362	−0.531	−0.530	0.699	0.001	1.057	0.759
	$C_3 - H$	1.09	0.276	−0.922	−0.718	−0.717	0.513	0.002	0.149	1.400
	$C_3 - H'$	1.09	0.276	−0.922	−0.718	−0.717	0.513	0.002	0.149	1.400
	$C_4 - H$	1.09	0.277	−0.923	−0.720	−0.719	0.515	0.001	0.147	1.396

Isomers refer to those in Fig. 2

γ-pyrane studied at the B3LYP/6–31G**//B3LYP/6–311++G** level gave the following values: ρ_b=0.254 a.u., $\nabla^2\rho_b$=−0.395 a.u., λ_1=−0.431 a.u., λ_3=0.461 a.u., $|\lambda_1|/\lambda_3$=0.941 and G_b/ρ_b=0.857 a.u., and ε=0.020 at BCP of O-1–C-2. At BCP of O-1–C-8a bond we found: ρ_b=0.280 a.u., $\nabla^2\rho_b$=−0.393 a.u., λ_1=−0.555 a.u., λ_3=0.708 a.u., $|\lambda_1|/\lambda_3$=0.775, G_b/ρ_b=1.050 a.u., and ε=0.017. Topological features of O1–C-8a BCP are a consequence of charge density redistribution over this molecular region, and could be related to lone pairs conjugation with closer π-orbitals. In fact, an important hyperconjugative charge transfer from both oxygen lone pairs (1n and 2n) into $\sigma_{C-8a-C-4a}$ and $\pi_{C-8a-C-4a}$ antibonding orbitals (1n→σ* and 2n→π*) can be observed by NBO analysis (Table 4; NBO second-order stabilisation energies, $E^{(2)}$, calculated at B3LYP/6–311++G** level are shown). Through a similar NBO analysis, the same resonance effect is also observed in benzo-2,3-dihydro-γ-pyrane, and twice in the pyrane molecule (where both C–O bonds have sp^2 carbon atoms). These results can be related to the origin of the λ_3 curvature increase (increase in the contraction extent of ρ(r) parallel to the bond, and from CP towards C-8a nuclei). Interestingly, through nuclear critical points (nCPs) analysis, this effect is correlated to a larger charge concentration over C-8a than over C-2. In fact, electron density is 119.620 a.u. at C-8a nCP, and 119.539 a.u. at C-2 nCP in Z-1. A Laplacian contour map of the electron density function accounting for the A ring plane is displayed in Fig. 3a. A slight asymmetry between O1–C-8a and O1–C-2 bonds in the inner contour line can be observed.

To describe the A, B and D rings, the difference in their features compared to those of the benzene ring will be useful. The values of the topological properties of C_2H_6 (ethane) and C_2H_2 (acetylene) will be also considered as references. Therefore, benzene, acetylene and ethane were also studied at the same calculation level (B3LYP/6–31G**//B3LYP/6–311++G**).

For Z-1 and Z-2, the electron charge density values of bond critical points (ρ_b) at C–C bonds of the A and B rings are between 0.305 a.u. and 0.310 a.u. with Laplacian values

Table 4 Main natural bond orbital (NBO) second-order stabilisation energies, $E^{(2)}$ calculated at B3LYP/6–311++G** level of theory, for $1,2n_{O1}$ and σ(O–C) donors

		Z-1	Z-2
Donor	Acceptor	$E^{(2)}$	
n/σ	σ*		
1O-1	C-8[a] —C-4[a]	7.15	7.12 [a]
1O-1	C-8[a] —C-8	0.56	0.54 [a]
1O-1	C-2—C-3	3.96	3.92 [a]
1O-1	C-2—C-1′	0.82	0.79 [a]
2O-1	C-2—C-1′	1.09	0.75 [a]
2O-1	C-2—C-3	1.67	1.67 [a]
2O-1	C-2—O	14.03	14.06 [a]
C-2—O-1	C-8[a] —C-8	2.26	2.32 [a]
C-2—O-1	C-3—H	1.03	1.15 [a]
C-2—O-1	C-1′—C-6′	1.93	1.41
C-2—O	C-1′—C-2′	1.93	1.41
C-8[a] —O-1	C-4[a]—C-5	1.75	1.77 [a]
C-8 [a] —O-1	C-8—C-7	1.33	1.33 [a]
C-8 [a] —O-1	C-2 —C1′	1.16	1.02 [a]

Isomers refer to those in Fig. 2. All values are expressed in kcal/mol
[a] Only bond interactions of A, B and C rings are displayed, but there is a symmetric contribution of bonds belonging to D and E rings

($\nabla^2\rho_b$) between −0.830 a.u. and −0.869 a.u. (ρ_b=0.308 a.u. and $\nabla^2\rho_b$=−0.854 a.u. for benzene). Ellipticity (ε) ranges from 0.202 to 0.249 for the A ring, and from 0.193 to 0.219 for the B ring (ε=0.200 for benzene). The former parameters (ρ_b and $\nabla^2\rho_b$) indicate that the C–C interactions are similar to those of benzene, some of them being slightly stronger and others slightly weaker. The latter parameter (ε) indicates that the π-character of these bonds is higher for the A ring than for the B ring or benzene. Therefore, the B ring is π-deficient with respect to the A and D rings, and will consequently be less reactive for electrophilic aromatic substitution. The other C–C single bonds belonging to the C and E rings show, at their BCPs, ρ_b values in the range of 0.240 a.u. and 0.251 a.u., and Laplacian values between −0.531 a.u. and −0.589 a.u.; ε values range from 0.010 to 0.032 (ρ_b=0.232 a.u., $\nabla^2\rho_b$=−0.505 a.u., and ε=0.000 for C_2H_6). This means that the C–C bonds are stronger than those of ethane, and have some π-character with respect to those of ethane. In fact, the C-3 atom yields the largest *p* contribution to the C-2–C-3 and C-3–C-4 bonds, as demonstrated by NBO analysis. For example, the contribution of C-3 atomic *p* orbitals in Z-1 to C-2–C-3, C-3–C-4 bonds is 74.08% and 72.61%, respectively; the contribution of C atom *p* orbitals to the C–C bond in C_2H_6 is 70.4%. These features can also be related to electron delocalisation due to hyperconjugative interactions, which will be discussed in the following paragraph.

The C–H bonds show ρ_b values between 0.276 a.u. and 0.283 a.u., and $\nabla^2\rho_b$ values between −0.922 a.u. and −0.980 a.u.. The C–H bonds of the A and D rings are stronger than the C-3–H and C-4–H bonds. The weakness of the latter bonds is related to their role as donors in hyperconjugative interactions. The main NBO second order energies associated with main charge transfer from $\sigma_{C-3—H}$ are shown in Table 5. These are mainly charge transferences into antibonding orbitals of bonds that are anti with respect to C-3–H bond (O-1–C-2, C-4–C-4a, O–C-2, and C-4–C-6″) and explain the increase in ellipticity in bonds that connect them (C-2–C-3 and C-3–C-4 bonds; Tables 2, 3). The second order energy of $\sigma_{C-H}\rightarrow\sigma^*_{C-O}$ transferences is higher than the energy of $\sigma_{C-H}\rightarrow\sigma^*_{C-C}$. Consequently, we found that the ellipticity of the C-2–C-3 bond is higher than that of the C-3–C-4 bond. These findings indicate that these hyperconjugative effects are responsible for the weakness of C-3–H and C-4–H bonds and electron delocalisation, thus giving rise to a π-character increase in C-2–C-3 and C-3–C-4 single bonds, as mentioned above.

Now we will describe A ring bonds for Z-1 and Z-2. As mentioned above, the increase in ellipticity of all bonds is significant with respect to the ellipticity of benzene C–C bonds (Tables 2, 3). This is interpreted as a π-character

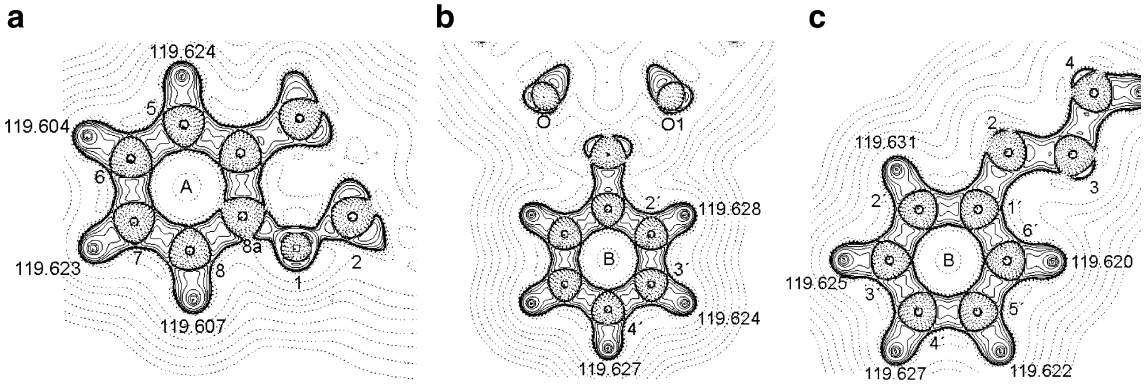

Fig. 3 Contour maps of the Laplacian of electron density of Z-1 in the planes of the A (**a**) and B (**b**) rings. The B ring of Z-2 is also shown (**c**). Electron densities values at (3,−3) critical points (CPs) over carbon nuclei are displayed. Atomic units are used

Table 5 Selected NBO second-order stabilisation energies, $E^{(2)}$ calculated at B3LYP/6–311++G** level of theory, for σ(C-3–H) and some σ(C–C) donors

		Z-1	Z-2
Donor	Acceptor	$E^{(2)}$	
σ	σ*		
C-3–H	C-2–O1	5.13	5.23[b]
C-3–H	C-4–C-4[a]	2.61	2.64[b]
C-2–C1′	C-1′–C2′	1.26	1.72
C-2–C1′	C1′–C6′	1.26	1.86
C-2–C1′	C2′–C3′	2.28	2.24
C-2–C1′	C6′–C5′	2.28	2.31
C-2–C1′	O1–C8 [a]	2.60	2.73[b]
C-2′–C-3′	C-4′–H	2.59	2.57
C-6′–C-5′	C-4′–H	2.59	2.62
C-2–C-3	C-1′–C-2′	0.67	2.71
C-2–C-3	C-1′–C-6′	0.67	–
C-1′–C-6′	C-2–O1	1.37	0.65

Relevant interactions related to σ*(C-4′–H) are also shown. Isomers refer to those in Fig. 2. All values are expressed in kcal/mol

[a] Only bond interactions of A, B and C rings are displayed

[b] Occurrence of a symmetric contribution of bonds belonging to D and E rings

enhancement of the bonds, which can be attributed to an enhancement in the extent of aromaticity of the A ring relative to benzene. On the other hand, although the A ring is benzenic, a loss of symmetry can be expected because of being bonded to a γ-pyrane moiety. In fact, taking into account bond lengths, C-8–C-7 and C-6–C-5 are shorter than the other bonds. C-4a–C-8a has the highest ellipticity (ε=0.249 for Z-1 and for Z-2), and thus the highest π-character. This feature is explained by a high NBO second order stabilisation energy (strong charge transference) for the $2n_O \rightarrow \pi^*_{C-8a-C-4a}$ interaction (26.30 kcal/mol in Z-1, and 26.70 kcal/mol in Z-2). The contributions of hyperconjugative interactions from the lone pairs ($1n_{O1}$ and $2n_{O1}$) of oxygen into C-8a–C-4a and C-8a–C-8 antibonding orbitals ($1,2n_{O1} \rightarrow \sigma^*_{C-8a-C-4a}$ and $1n_{O1} \rightarrow \sigma^*_{C-8a-C-8}$), and from C-2–O1 bond orbital into C-8a–C-8 antibonding orbitals ($\sigma_{C-2-O1} \rightarrow \sigma^*_{C-8a-C-8}$) are shown in Table 4. Transferences from C-8a–O-1 into C-4a–C-5 and C-8–C-7 antibonding orbitals ($\sigma_{C-8a-O1} \rightarrow \sigma^*_{C-4a-C-5}$ and $\sigma_{C-8a-O1} \rightarrow \sigma^*_{C-8-C-7}$) are also included. The $\sigma_{C-8a-O1} \rightarrow \sigma^*_{C-4a-C-5}$, $1n_O \rightarrow \sigma^*_{C-8a-C-4a}$ and $1n_O \rightarrow \sigma^*_{C-8a-C-8}$ interactions led to an increase in population of the corresponding acceptor antibonding orbitals, thus giving rise to elongated C4a-C5 (with respect to C8-C7), C8–C8a and C8a–C4a bonds. A $\sigma_{C-8a-O1} \rightarrow \sigma^*_{C-8-C-7}$ transference also occurs, but the energy is less than that of the $\sigma_{C-8a-O1} \rightarrow \sigma^*_{C-4a-C-5}$ transference. Consequently, the C-8–C-7 bond is shorter than the C-8a–C-4a bond. Throughout these mechanisms, the oxygen atom provides electron density to the A and D rings, and would produce an increase in charge concentration at C-7 and C-5. In fact, via analysis of nCPs, we found larger electron density values (119.623 a.u.) at C-5 and C-7 nuclei (density values on nCPs for the A ring are shown in Fig. 3a). These results would show activation at the 5 and 7 positions with respect to aromatic electrophilic substitution, which in fact has been verified experimentally by the synthesised substituted structures [1] (Fig. 4).

The B ring of Z-1 is significantly different from that of Z-2; therefore, it will be described separately. Due to the effect of both γ-pyrane moieties (A-C and D-E rings), a loss of symmetry in the B ring is observed for Z-1 related to benzene symmetry. The C-1′–C-2′ and C-1′–C-6′ bonds have higher ellipticity (π-character) than those of benzene (ε=0.207). The remaining bonds are shorter and have a lower ellipticity (π-character) than those of benzene.

Second order energies revealed by NBO analysis show that there are important charge transferences from the C-2–C-1′ bond to the C-1′–C-2′, C-1′–C-6′, C-2′–C3′ and C6′–C5′ antibonding orbitals (Table 5). The former values support the higher length of the C-1′–C-2′ and C-1′–C-6′ bonds, the others explain the higher ellipticities (π-character) of C-1′–C-2′ and C-1′–C-6′. Another interesting transference occurs from both C-2′–C3′ and C6′–C5′ bonding orbitals to the C-4′–H antibonding orbital. These results indicate a reinforcement of hyperconjugative interactions, thus giving rise to electron delocalisation over the para position of the B ring, and would produce an increase in C-4′ charge concentration. In fact, in studying the nCPs of the B ring carbon atoms we found a larger electron density (119.627 a.u.) in C-4′ than in any other carbon atoms [119.624 a.u. over C-3′ (meta); Fig. 3b]. These results show that a para aromatic electrophilic substitution in the B ring is favoured, in agreement with experimental results, e.g. synthesised substituted structures (Fig. 4). Ortho substitution (119.628 a.u., over C-2′) would be prevented by steric hindrance.

The B ring of Z-2 also loses the symmetry found in benzene, thus C-2′–C-3′ and C-4′ –C-5′ are shorter than C–

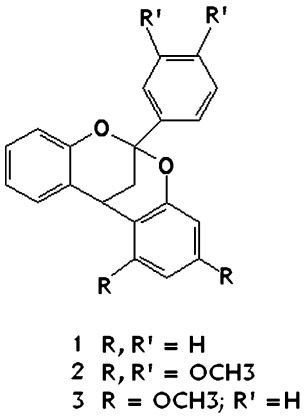

Fig. 4 Structures of substituted A-type dimeric proanthocyanidins

C in benzene. From the nPC analysis of carbon atoms we found para activation also in Z-2 (Fig. 3c). Transferences from C-2′–C-3′ and C-6′–C-5′ bonding orbitals into the C-4′–H antibonding orbital are similar to those in Z-1 (Table 5). Therefore, the highest electron density found at C-4′ is explained by two hyperconjugative interactions that operate in a coordinate way as in Z-1. Evidently, for these interactions, B ring rotation when going from Z-1 to Z-2 has no major effects. Density values on C-2′ and C-3′ nuclei (mainly the former) are important (Fig. 3c), but these values now arise from another source: hyperconjugative interactions between C–C single bonds of the D and E rings with those of the B ring. In particular, the $\sigma_{C-2-C-3} \rightarrow \sigma^*_{C-1'-C-2'}$ transference (Table 5) in Z-2 is one order of magnitude higher than that in Z-1 (in Z-2, C-3–C-2 is anti with respect to C-1′–C-2′). All these results explain para activation at the C-2′ and C-3′ positions for the B ring in Z-2.

Molecular electrostatic potential maps

Electrostatic potential V(r) is suitable for studying processes based on the ‘recognition’ of one molecule by another, such as drug–receptor, and enzyme–substrate interactions, because it is through these potentials that both species ‘see’ each other. Molecular electrostatic potentials [27, 28] have been primarily used for predicting sites, relative reactivities towards electrophilic attack, biological recognition and hydrogen bonding interactions. Because it is a real physical property, V(r) can be determined either experimentally by diffraction or by computational methods [29]. In this paper, we use the approach first proposed by Politzer et al. [30–33] for electrostatic potentials [34].

These studies focused on negative regions of V(r). MEP maps can be useful in understanding sites for electrophilic attack [35]. In most MEPs, regions of negative values account for local minima and are site candidates for electrophilic attack [27].

MEP maps for rotamers of the *Z*-isomers, Z-1 and Z-2, of A-type proanthocyanidin, in a.u., are shown in Fig. 5. These species have two sites for electrophilic attack that are very close to each other, thus giving rise to the type of large region preferred for this kind of attack, in which V(r) calculations provide insights into preference order. The 3D electrostatic potential contour map shows that negative regions are associated with oxygen atoms. Over them, V(r) values are −0.13081 a.u. for Z-1 and −0.12589 a.u. for Z-2. These values allow us to state that the Z-1 conformer will be more reactive than Z-2, thus indicating oxygen’s tendency to be involved in electrostatic interactions, ion-pair formation or hydrogen bonding, which will be important in the antioxidant role of proanthocyanidin. In future studies on substituted molecules, it will be of great importance to relate oxygen V(r) values, taking into account values determined on simple structures.

The highest values of V_{min} in Z-1 would mean that inductive effects exerted by oxygen atoms are more intense in Z-1. NBO analysis allowed us to corroborate this hypothesis by studying bond polarisation [36]. In fact, we can conclude that C-6′–C-1′ and C-1′–C-2′ bonds are more polarised in Z-1 than in Z-2. Thus, for the C-6′–C-1′ bond in Z-1, we found 51.08% (50.44% in Z-2) of electron density on C-6′, and 48.92% (49.56% in Z-2) of electron density on C-1′, thus indicating a stronger inductive effect in Z-1 than in Z-2.

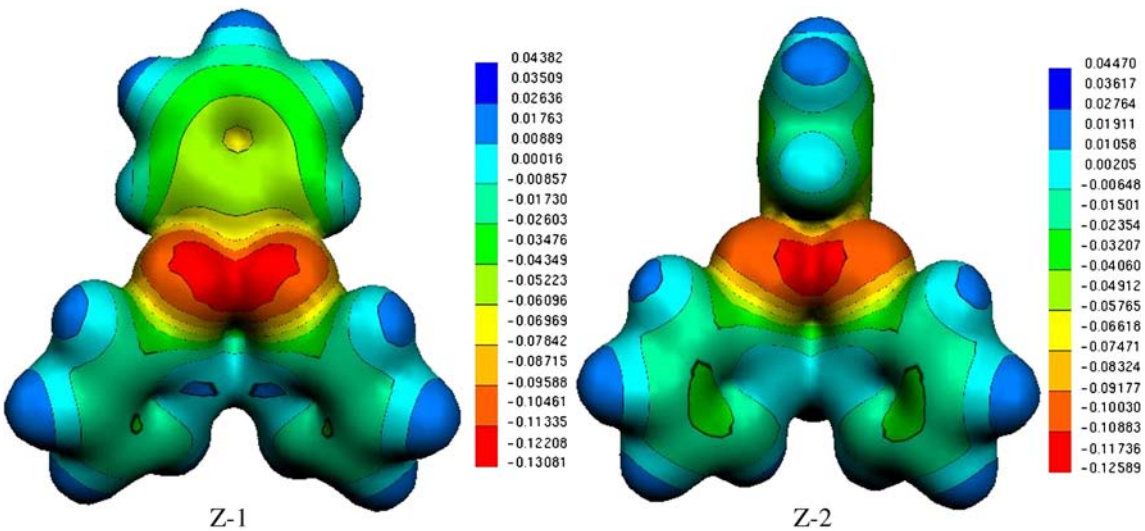

Fig. 5 Maps of molecular electrostatic potential (MEP) for the Z-1 and Z-2 rotamers, and the *E*-isomer of unsubstituted A-type dimeric proanthocyanidin. Values in a.u.

Topology of Laplacian of the electronic charge density function

Once reactive sites have been localised on the basis of MEPs, the non-bonded (3,−3) critical points (NBCPs) of the Laplacian of the electronic charge density function were studied. NBCPs were determined on oxygen atoms, where the highest values of V_{min} were encountered. We found two NBCPs in the valence shell of each O atom, one above and another below the plane defined by the A ring ($\nabla^2\rho_{nb}$= −5.019 a.u., r=0.6455 a.u. and $\nabla^2\rho_{nb}$=−4.996 a.u., r= 0.6457 a.u. for Z-1; and $\nabla^2\rho_{nb}$=−5.037 a.u., r=0.6453 a.u. and $\nabla^2\rho_{nb}$=−4.970 a.u., r=0.6459 a.u. for Z-2). This fact supports the occurrence of two electron pairs of a sp^3 oxygen atom, as mentioned above. These NBPCs allowed us to localise the oxygen lone pairs in the actual space, forming an angle, e.g. 110.1° for Z-1 and 109.0° for Z-2, with respect to the oxygen atom. Hybridization of these lone pairs is in line with the conjugation of these electrons with the A, B and D aromatic rings. We found that the lone pair above the plane ($1n_O$, in Table 4) is 36.92% *s* and 63.05% *p* in Z-1 (37.23% *s* and 62.74% *p* in Z-2) by NBO analysis. The lone pair below the plane ($2n_O$) is 99.95% *p* in Z-1 (99.96% *p* in Z-2). The highest angle between the lone electron pairs and the minor NBCP($1n_O$)–O-1–C-2–C-1′ dihedral angle (32.51 in Z-1 and 35.15 in Z-2) can be related to a more effective conjugation of oxygen lone pairs in Z-1 than in Z-2. Optimised structures are shown in Fig. 6. The spatial position of NBCPs accounting for O-1 is also included. A ring is perpendicular to the plane, and the O-1 atom is just behind C-2, as shown in Fig. 6a, thus only the lone pairs are visible ($1n_{O1}$ and $2n_{O1}$). Our results show that lone pairs tend to line up to C-2–C-1′ to maximise hyperconjugative effects. In fact, from NBO analysis we can see (Table 4) that $2, 1n_O \rightarrow \sigma^*_{C-2-C-1'}$ transferences are 24% stronger in Z-1 than in Z-2. This effect is also related to the fact that the C-3–C-2–C-1′ angle is less in Z-1 than in Z-2.

NMR study

Experimental and calculated [B3LYP/6−31G(d,p)] NMR chemical shifts (δ) of unsubstituted A-type dimeric proanthocyanidin are shown in Table 5. The spectrum was recorded on Bruker HFX 90 (90 MHz for ^{1}H-NMR; 22.63 MHz for ^{13}C-NMR) equipment in $CDCl_3$ with TMS as an internal reference. Experimental values show the presence of the intramolecular plane of symmetry, since the following equivalences were found: C-8a/C-1″, C-8/C-2″, C-7/C-3″, C-6/C-4″, C-5/C-5″ and C-4a/C-6″. These measurements are in agreement with the molecular characteristics found in the optimised structures. The calculated chemical shifts show the same trends as the measured ones (Table 6). Symmetry was also found experimentally between C-2′ and C-6′ as well as between C-3′ and C-5′. These features were theoretically found only for Z-1, which is also the conformer with the lowest energy. Therefore, the experimental NMR spectrum of unsubstituted A-type dimeric proanthocyanidin accounts for the most stable conformer according to calculations. Furthermore, this result means that the most thermodynamically stable conformer is also the most kinetically stable one.

Taking into account the theoretical results, the effect of B ring rotation on chemical shifts can be observed. Oxygen atoms are more shielded in Z-1 (30.51 ppm) than in Z-2 (41.25 ppm), the O-1–C-2–C-1′–C-2′ dihedral angle being 33.52° for Z-1 and 93.31° for Z-2. C-3, C-2 and C-6′ of Z-2 are clearly more shielded than those of Z-1. However, C-2′ is more deshielded in Z-2 than in Z-1, and also more than C-6′. In this case, the B ring rotates approximately 80° around the C-2/C-1′ bond as mentioned above, and the C-3–C-2–C-1′ - C-6′ dihedral angle is 0.001° (88.16° for Z-1). In other words, for Z-1 both C-2′ and C-6′ are located in equivalent magnetic environments, but when the B ring rotates to achieve Z-2, C-6′ is shielded, while C-2′ is deshielded. We found that these characteristics are related

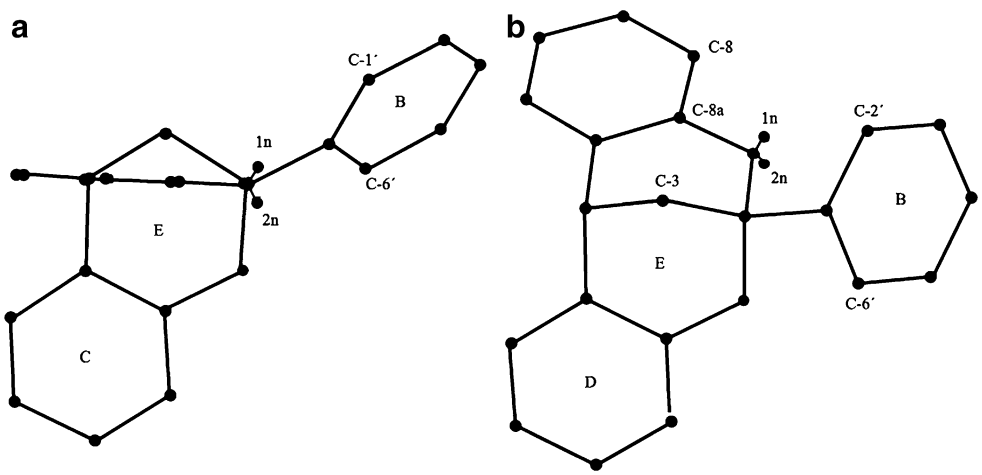

Fig. 6 Optimised geometry of the Z-1 conformer. Non-bonded (3,−3) critical points (NBCPs) accounting for lone pairs of oxygen atoms are shown (1n and 2n)

Table 6 Experimental ^{13}C-NMR chemical shifts (δ) of unsubstituted A-type dimeric proanthocyanidin, and calculated [B3LYP/6–31G(d,p)] chemical shifts

C atom	Z-1 Calculated	Experimental	Z-2 Calculated	C atom	Z-1 Calculated	Experimental	Z-2 Calculated
2	107.52	99.06	106.06				
3	42.26	35.03	35.20				
4	44.79	33.95	44.00				
5	128.66	126.01	128.47	1″	154.16	152.53	153.48
6	121.95	121.70	121.70	2″	118.18	117.07	118.16
7	129.04	127.41	128.95	3″	129.04	127.41	128.94
8	118.18	117.07	118.16	4″	121.95	121.70	121.71
8a	154.16	152.53	153.48	5″	128.66	126.01	128.47
4a	129.55	126.88	129.31	6″	129.55	126.88	129.31
1′	144.35	142.18	144.00				
2′	128.08	128.28	130.77				
3′	129.02	128.60	129.77				
4′	129.28	128.92	129.43				
5′	129.02	128.60	127.94				
6′	128.08	128.28	123.11				

Isomers refer to those in Fig. 2. δ in ppm

to electron density values at the corresponding nuclear CPs: higher values account for deshielded nuclei (Fig. 3c). As expected, for C-5 and C-6 or C-7 atoms of the A ring, the same trend was observed: higher electron density over nuclei is related to higher deshielding (Fig. 3a). The hyperconjugative effects mentioned above, which explain electron density accumulation over C-2′ in Z-2, and over C-5, C-6 and C-7 could also allow their relative deshielding.

Spin-spin coupling constants were also calculated, giving rise to an interesting information. Upon comparison of Z-1 and Z-2, similar calculated values are observed, except for ^{2}J(C-1′,O), which is ca. 5 Hz higher for Z-1 than for Z-2 (−10.67 Hz and −6.38 Hz, respectively). This coupling largely obeys the Fermi contact (FC) mechanism (−10.74 Hz and −6.36 Hz, respectively). We can expect that $1,2n_{O1} \rightarrow \sigma^{*}_{C-2-C-1'}$ hyperconjugative interactions (and symmetric ones) mainly affect this coupling constant [37]. In fact, by NBO analysis we could see that there are hyperconjugative interactions that introduce charge into antibonding C-2–C-1′ (which are 20% stronger in Z-1 than in Z-2; Table 4), thus yielding a positive increase to the FC contribution to ^{2}K(C-1′,O) reduced spin-spin coupling constant, as the FC term is sensitive to electrons in *s* orbitals [38]. Furthermore, we found other hyperconjugative interactions that transfer charge over antibonding C-2–O1 in a more effective way in Z-1, e.g. second order energy for $\sigma_{C-1'-C-6'} \rightarrow \sigma^{*}_{C-2-O1}$ charge transfer is 1.37 kcal/mol in Z-1 and 0.65 kcal/mol in Z-2 (Table 5). These results show how useful the ^{2}J(C-1′,O) geminal spin-spin coupling is as a probe to analyse stereochemical aspects in organic compounds, as has been recently reported [R.H. Contreras et al. manuscript submitted]. More in depth studies on coupling pathways, their sensitivity to hyperconjugative interactions and the stereochemical dependence of NMR geminal ^{2}J(C-1′,O) as well as vicinal ^{3}J(C-2′,O) spin-spin coupling constants in A-type proanthocyanidins are in progress in our laboratories.

Conclusions

A knowledge of the electronic structure of the unsubstituted type-A dimeric proanthocyanidin, its stereochemistry and the effects involved will have pivotal value as reference basis for further studies on substituted and complex proanthocyanidins.

The occurrence of a rigid substructure with high π-character in the A-type proanthocyanidin led to *E*/*Z*-isomerism. The *Z*-isomer was more stable than the *E*-isomer. Two rotamers, Z-1 and Z-2, were obtained for the *Z*-isomer.

The conformational space of A-type proanthocyanidin stereoisomers was scanned using MD at the semiempirical level, and further density calculations were performed. The electronic distributions of the lowest energy conformers Z-1 and Z-2 were analysed further at a higher calculation level, thus improving the basis set; a topological study in Bader's theory framework was performed and hyperconjugative interactions were analysed with an NBO approach. MEP maps were obtained and analysed. NMR chemical shifts were calculated at ab initio level and compared with experimental values; coupling constants were also calculated.

The rigid [3.1.3]bicyclic substructure containing the CH_2-3 bridge supported the π-character of C-2–C-3 and

C-3–C-4 bonds, which was demonstrated by electron charge density calculations and NBO analysis.

Our findings demonstrate that the oxygen atom shows two lone electron pairs, one above and another below the plane defined by the A ring, which corresponds to an sp^3 oxygen atom. This fact can be related to the effective conjugation of the π-system of the A and D aromatic rings. One of the lone pairs (labeled 1n and localised above the plane of the molecule) is of *sp*-type and the other (labeled 2n and localised below the plane of the molecule) is of the *p*-type. Each one plays a critical role. The second lone pair is involved in the strongest interaction with the A ring π-system and in the interactions that connect the D and E rings. In other words, 2n is associated mainly with the steric arrangement of the A, C, D and E rings. The first, 1n, is instead especially sensitive to B ring spatial orientation with respect to the rest of the molecule, thus showing improved electron delocalisation in Z-1, which is related mainly to the higher stability of that conformer. By NBO analysis, we draw the conclusion that oxygen lone pairs and C–O bonding orbitals are involved in hyperconjugative interaction, thus transferring charge to different rings and bonds, and these transferences are stronger in Z-1 than in Z-2. Therefore, we can relate the higher stability of Z-1 to enhanced electron delocalisation. For example, $LP \rightarrow \sigma^*_{C-2-C-1'}$, $\sigma_{C-2-O1} \rightarrow \sigma^*_{C-1'-C-6'}$ and $\sigma_{C-2-O} \rightarrow \sigma^*_{C-1'-C-2'}$ interactions are stronger for Z-1 than for Z-2.

Larger delocalization effects on Z-1 can be also related to larger bond ellipticity, which, by hyperconjugative interactions, gives rise to electron charge delocalisation on those bonds, thus increasing their π-character. According to the examples shown above, the first transference gives rise to an increased O1–C-2 bond ellipticity for Z-1 with respect to Z-2, and the others explain the increased C-2–C1′ bond ellipticity for Z-1 with respect to Z-2.

According to our results, both C-8a–O and O–C-2 covalent bonds have topologically distinctive features, which depend on carbon hybridisation. There are hyperconjugative interactions involving oxygen atoms of the E and C rings, which are responsible for those differences increasing the extent of contraction of electron density parallel to the C-8a–O bond, and from the critical point towards C-8a nuclei, thus increasing electron density over these nuclei.

We also found geometric evidence to explain a more effective conjugation of lone pairs over the molecule: a larger angle between lone pairs, and better overlapping between 1n and the C-2–C-1′ bond. The behaviour of V_{min} can also be rationalised by NBO and AIM analysis, and we can conclude that their highest values and the large extension of the zone of high negative values for Z-1 can be associated with more efficient electron-withdrawing mechanisms (inductive effect). In other words, we found a stronger inductive effect in Z-1, but previously we also found stronger hyperconjugative effects in the same compound. Therefore, throughout this work we have demonstrated that, in the lowest energy conformer of A-type proanthocyanidin, the polar effect exerted by the oxygen of pyrane rings over the B ring is a coordinative combination of both kinds of effects, which increase in a combined manner. In other words our results indicate that a "resonance assisted" inductive effect, which reaches a maximum when the structure reaches the minimum energy, is operating.

These results also reveal a relationship between hyperconjugative transferences and densities over some nuclear critical points and ellipticities at some bond critical points, which allows us to compare aromaticities between aromatic rings and preference order for aromatic electrophilic attack. Thus, the B ring is less reactive with respect to aromatic electrophilic substitution than the A or D rings. Moreover, we showed that pyrane rings behave as para (preferentially) and meta activators in reactions of aromatic electrophilic substitution of the B ring in Z-1. Likewise, we also conclude that the 2,3 fusion (C-4a/C-8a) of the γ-pyrane ring to the A ring activates C-5 and C-7 sites (and equivalent positions on the D ring: C-5″ and C-3″). Geometrical asymmetries of the A and D rings have been also explained by AIM parameters together with hyperconjugative interactions, transferring charge into some antibonding orbitals, thus producing bond enlargements.

Using both theoretical and experimental NMR studies, we have shown that the NMR spectrum of A-type proanthocyanidin accounts for the most stable conformer according to calculations. Furthermore, this means that the most thermodynamically stable conformer is the same as the most kinetically stable one. On the other hand, the theoretical results can demonstrate the effect of rotation of the B ring on chemical shifts, and, furthermore, ^{13}C chemical shifts (δ) can be a very useful tool to determine the spatial orientation of the B ring with respect to the rest of the molecule. Also, the ^2J(C-1′,O) coupling constant is significant in the description and understanding of the stereochemistry of proanthocyanidins.

A useful coordination of AIM and NBO analyses, and the key role of hyperconjugative interactions in defining experimental trends, have been demonstrated in this study. Increased ellipticities (increased π-character) are related to hyperconjugative transferences, thus showing that enhanced density at nuclear critical points of carbon atoms of aromatic rings has the same origin and can be related to deshielding of the corresponding nuclei, and thus can be used as an indicator of active sites for electrophilic attack.

This work constitutes the first step towards our aim of rationalising the action of these compounds on juice stabilisation by attempting to elucidate deeper insights into

the physicochemical properties and effects of flavonoids on oxidative processes. Experimental and theoretical study of the structure of substituted compounds are in progress in our laboratories.

Acknowledgements Thanks are due to CONICET, Universidad Nacional de La Plata and Universidad de Buenos Aires (Argentina) for financial support. One of us (A.B.P.) is a Senior Research Member of the National Research Council of Argentina (CONICET). A.H.J. is a Member of the Scientific Research Career (CIC, Provincia de Buenos Aires). R.M.L. acknowledges Universidad de la Cuenca del Plata (Corrientes, Argentina) for facilities provided during the course of this work.

References

1. Pomilio A, Müller O, Schilling G, Weinges K (1977) Zur Kenntnis der Proanthocyanidine, XXII. Über die Konstitution der Kondensationsprodukte von Phenolen mit Flavyliumsalzen. Justus Liebigs Ann Chem, 597–601. doi:10.1002/jlac.197719770409
2. Ricardo da Silva JM, Darmon N, Fernandez Y, Mitjavilla S (1991) Oxygen free radical scavenger capacity in aqueous models of different procyanidins from grape seeds. J Agric Food Chem 39:1549–1552. doi:10.1021/jf00009a002
3. Liu ZQ, Ma LP, Zhou B, Yang L, Liu ZL (2000) Antioxidative effects of green tea polyphenols on free radical initiated and photosensitized peroxidation of human low density lipoprotein. Chem Phys Lipids 106:53–63. doi:10.1016/S0009-3084(00)00133-X
4. Liu L, Xie B, Cao S, Yang E, Xu X, Guo S (2007) A-type procyanidins from *Litchi chinensis* pericarp with antioxidant activity. Food Chem 105:1446–1451. doi:10.1016/j.foodchem.2007.05.022
5. Kedage VV, Tilak JC, Dixit GB, Devasagayam TPA, Mhatre M (2007) A study of antioxidant properties of some varieties of grapes (*Vitis vinifera* L.). Crit Rev Food Sci Nutr 47:175–185. doi:10.1080/10408390600634598
6. Pinent M, Bladé C, Salvadó MJ, Blay M, Pujadas G, Fernandez-Larrea J, Arola L, Ardevol A (2006) Procyanidin effects on adipocyte-related pathologies. Crit Rev Food Sci Nutr 46:543–550. doi:10.1080/10408390500354537
7. Pomilio A, Ellmann B, Künstler K, Schilling G, Weinges K (1977) Naturstoffe aus Arzneipflanzen, XXI. ^{13}C-NMR-spektroskopische Untersuchungen an Flavanoiden. Justus Liebigs Ann Chem, 588–596. doi:10.1002/jlac.197719770408
8. Ditchfield R, Miller DP, Pople JA (1970) Molecular orbital theory of carbon NMR chemical shifts. Chem Phys Lett 6:573–575. doi:10.1016/0009-2614(70)85229-0
9. Gelius U, Roos B, Siegbahn P (1970) Ab initio MO SCF calculations of ESCA shifts in sulphur-containing molecules. Chem Phys Lett 4:471–475. doi:10.1016/0009-2614(70)85018-7
10. Ditchfield R (1972) On molecular orbital theories of NMR chemical shifts. Chem Phys Lett 15:203–206. doi:10.1016/0009-2614(72)80149-0
11. Kaupp M, Malkin VG, Malkina OL, Salahub DR (1996) Ab initio ECP/DFT calculation and interpretation of carbon and oxygen nmr chemical shift tensors in transition-metal carbonyl complexes. Chem Eur J 2:24–30. doi:10.1002/chem.19960020108
12. Schindler M, Kutzelnigg W (1983) Theory of magnetic susceptibilities and NMR chemical shifts in terms of localized quantities. 3. Application to hydrocarbons and other organic molecules. J Am Chem Soc 105:1360–1370. doi:10.1021/ja00343a049
13. Gauss J (1993) Effects of electron correlation in the calculation of nuclear magnetic resonance chemical shifts. J Chem Phys 99:3629–3643. doi:10.1063/1.466161
14. van Wüllen CJ (1995) Chem Phys 102:2806–2811. doi:10.1063/1.468657
15. Bader RFW (1990) A quantum theory of molecular structure and its applications. Chem Rev 91:893–928. doi:10.1021/cr00005a013
16. Bader RFW (1995) Atoms in molecules. A quantum theory. Oxford University Press, Oxford
17. Popelier P (2000) Atoms in molecules. An introduction. Prentice Hall
18. HyperChem Release 7.5, Hypercube Inc., USA
19. Gaussian 98, Revision A.7, Frisch MJ, Trucks GW, Schlegel HB, Scuseria GE, RobbMA, Cheeseman JR, Zakrzewski VG, Montgomery JA Jr, Stratmann RE, Burant JC, Dapprich S, Millam JM, Daniels AD, Kudin KN, Strain MC, Farkas O, Tomasi J, Barone V, Cossi M, Cammi R, Mennucci B, Pomelli C, Adamo C, Clifford S, Ochterski J, Petersson GA, Ayala PY, Cui Q, Morokuma K, Malick DK, Rabuck AD, Raghavachari K, Foresman JB, Cioslowski J, Ortiz JV, Baboul AG, Stefanov BB, Liu G, Liashenko A, Piskorz P, Komaromi I, Gomperts R, Martin RL, Fox DJ, Keith T, Al-Laham MA, Peng CY, Nanayakkara A, Gonzalez C, Challacombe M, Gill PMW, Johnson B, Chen W, Wong MW, Andres JL, Gonzalez C, Head-Gordon M, Replogle ES, Pople JA (1998) Gaussian, Inc., Pittsburgh PA.
20. Becke AD (1993) Density-functional thermochemistry. III. The role of exact exchange. J Chem Phys 98:5648–5652. doi:10.1063/1.464913
21. Lee C, Yang W, Parr RG (1988) Development of the Colle-Salvetti correlation energy formula into a functional of the electron density. Phys Rev B 37:785–789. doi:10.1103/PhysRevB.37.785
22. Flúkiger P, Lúthi HP, Portmann S, Weber J (2000) MOLEKEL 4.0. Swiss Center for Scientific Computing, Manno, Switzerland
23. Biegler-König FW, Bader RFW, Tang TH (1982) Calculation of the average properties of atoms in molecules. II. J Comput Chem 3:317–328. doi:10.1002/jcc.540030306
24. Glendening ED, Reed AE, Carpenter JE, Weinhold F NBO 3.1. Program as implemented in the Gaussian 98 package
25. Becke AD, Edgecombe KE (1990) A simple measure of electron localization in atomic and molecular systems. J Chem Phys 92:5397–5403. doi:10.1063/1.458517
26. Bader RFW (1998) A bond path: a universal indicator of bonded interactions. J Phys Chem A 102:7314–7323. doi:10.1021/jp981794v
27. Politzer P, Laurence PR, Jayasuriya K (1985) Molecular electrostatic potentials: an effective tool for the elucidation of biochemical phenomena. Environ Health Perspect 61:191–202. doi:10.2307/3430072
28. Politzer P, Murray JS (1991) In: Beveridge DL, Lavery R (eds) Theoretical biochemistry and molecular biophysics: a comprehensive survey, vol 2, protein. Adenine, Schenectady, NY, Chapter 13
29. Politzer P, Truhlar DG (eds) (1981) Chemical applications of atomic and molecular electrostatic potentials. Plenum, New York
30. Politzer P, Landry SJ, Waernheim T (1982) Proposed procedure for using electrostatic potentials to predict and interpret nucleophilic processes. J Phys Chem 86:4767–4771
31. Politzer P, Abrahmsen L, Sjoberg P (1984) Effects of amino and nitro substituents upon the electrostatic potential of an aromatic ring. J Am Chem Soc 106:855–860
32. Politzer P, Laurence PR, Abrahmsen L, Zilles BA, Sjoberg P (1984) Chem Phys Lett 111:75–78
33. Murray JS, Lane P, Brinck T, Politzer P, Sjoberg P (1991) Electrostatic potentials on the molecular surfaces of cyclic ureides. J Phys Chem 95:844–848
34. Bader RFW (1990) Chem Rev 91:893–928. doi:10.1021/cr00005a013

35. Muñoz-Caro C, Niño A, Sement ML, Leal JM, Ibeas S (2000) Modeling of protonation processes in acetohydroxamic acid. J Org Chem 65:405–410
36. Alabugin IV, Manoharan M, Peabody S, Weinhold F (2003) Electronic basis of improper hydrogen bonding: a subtle balance of hyperconjugation and rehybridization. J Am Chem Soc 125:5973–5987
37. Tormena CF, Rittner R, Contreras RH, Peralta JE (2003) Theoretical calculation of proto-proton NMR indirect spin-spin coupling constants in heterocyclic three-membered rings. Ann Magn Reson 2:70–72
38. Contreras RH, Peralta JE (2000) Angular dependence of spin-spin coupling constants. Prog Nucl Magn Reson Spectrosc 37:321–425. doi:10.1016/S0079-6565(00)00027-3